Chinese Chemical Letters 34 (2023) 107851

Contents lists available at ScienceDirect

Chinese Chemical Letters

journal homepage: www.elsevier.com/locate/cclet

Designing polyoxometalate-based metal-organic framework for oxidation of styrene and cycloaddition of CO_2 with epoxides

Xiaomei Yan[a], Jiangbo Xu[a], Ting Zhang[a], Chen Si[a], Jiachen Jiao[a], Jie Li[b], Qiuxia Han[a,*]

[a] Henan Key Laboratory of Polyoxometalate Chemistry, School of Chemistry and Chemical Engineering, Henan University, Kaifeng 475004, China
[b] School of Chemistry & Chemical Engineering, Zhoukou Normal University, Zhoukou 466001, China

ARTICLE INFO

Article history:
Received 28 July 2022
Revised 22 August 2022
Accepted 22 September 2022
Available online 27 September 2022

Keywords:
Polyoxometalate
Metal-organic framework
Photocatalysis
Oxidation of styrene
Cycloaddition

ABSTRACT

A photoactive polyoxometalate-based metal−organic framework (POMOF), NiW-DPNDI, was synthesized by combination of Ni(II) ions, $[ZnW_{12}O_{40}]^{6-}$ anions, and *N,N'*-bis(4-pyridylmethyl)naphthalene diimide (DPNDI) molecules into one single framework. NiW-DPNDI displays a three-dimensional structure by the strong anion$\cdots\pi$ interactions between the trapped $[ZnW_{12}O_{40}]^{6-}$ anions and the electron-deficient naphthalenic ring centroids and the $\pi-\pi$ stacking interactions between DPNDI moieties. NiW-DPNDI displayed a highly efficient hole-electron separation and ordered electron transfer under irradiation, thus ensuing its excellent photocatalysis in oxidation of styrene to produce benzaldehyde. In addition, it gave a high efficiency for styrene oxide under thermocatalytic conditions. Because the carbonic anhydrase (CA)-mimicking Ni sites and the negative electron-enriched $[ZnW_{12}O_{40}]^{6-}$ anions are well aligned in the pores, it can promote the cycloaddition of CO_2 with epoxides under mild conditions.

Nowadays, the efficient conversion of hydrocarbons derived from fossil fuel resources into high additional-value compounds by selectivity oxidation has been become one of the most important reactions of modern petrochemical industry [1–5]. Benzaldehyde and styrene oxide are important intermediates of pharmaceutical, pesticide and functional materials, which can be produced by selective oxidation of styrene [6–8]. Photocatalytic oxidation technology is receiving considerable attention as one of the most promising strategies to obtain compounds for having an inherent advantage in environmental protection, energy conservation and high efficiency by utilizing environmentally singlet oxygen ($^1O_2$) and solar energy source to drive the redox reaction [9–12]. However, as a sole oxidant $^1O_2$, its reaction efficiency still needs to be improved. Superoxide radicals ($O_2^{\cdot-}$) has displayed excellent catalytic performance in many reactions, which can be produced by heterogeneous photocatalysts through photogenerated electrons transferring to O_2 [13–15]. Therefore, in order to achieve the synergy of $^1O_2$ and $O_2^{\cdot-}$, it is imperative to develop charge transfer units and to promote multi-electron transfer reactions.

The combination of photosensitizer and oxidation catalyst within one framework has attracted much attention as a powerful generation photocatalysts for prospective practical applications [16–18]. Beyond that, the major challenge to achieve high photocatalytic efficiency and selectivity lies in the synergy of the multiple catalytic sites and the efficient electron transfer. Inspired by the high efficient, specificity and stereoselective of natural enzymes, chemists have attempted to construct chemical photocatalysis system capable of forming long-lived charge-separated states for advances in solar energy conversion [19–21]. By assembling the well-chosen electron donor and acceptor in an analogous coordination mode to metalloenzymes make them possess highly intrinsic peroxidase-like activity, good stability and long excited state lifetimes [22,23].

Functional naphthalenediimide (NDI) derivatives as n-type semiconductors meet the evaluation of design principles because of their efficient electron-transfer properties, high redox activity and strong π-acidity [24,25]. Additionally, it can be easily introduced into framework by using non-covalent or covalent strategies to enhance the light absorption capacity of catalysts act as a photosensitizer. Owing to the excellent reversible photo- and electro-chromism, thermal stability and redox-active properties, polyoxometalates (POMs) are well-known catalysts studied in the olefin epoxidation [26,27]. Especially for multi-electron transfer processes, POMs are promising candidates because they are stable against oxidative degradation and can receive a lot of electrons and protons without deforming their structures [28–30].

In this context, a new polyoxometalate-based metal-organic framework (POMOF), $Ni_2(H_2O)_7(DPNDI)_{2.5}$ $[H_2ZnW_{12}O_{40}]\cdot 2H_2O$

* Corresponding author.
E-mail address: hdhqx@henu.edu.cn (Q. Han).

https://doi.org/10.1016/j.cclet.2022.107851
1001-8417/

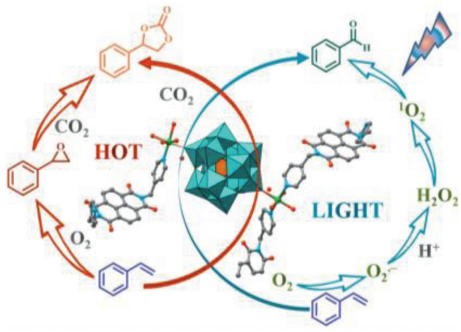

Scheme 1. The design concept of NiW-DPNDI for photocatalysis styrene oxidation.

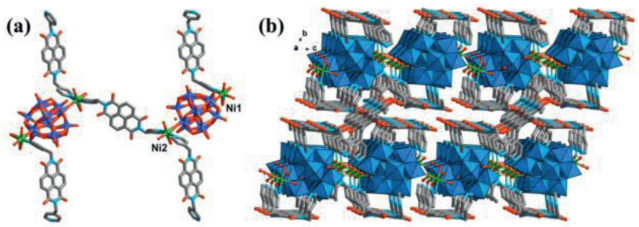

Fig. 1. (a) Ball-and-stick representation of NiW-DPNDI. (b) 3D open network of NiW-DPNDI viewed down the *a* axis.

(NiW-DPNDI) was synthesized by solvothermal method in presence of nickel(II) ion, $[WZn_3(H_2O)_2(ZnW_9O_{34})_2]^{12-}$ and DPNDI ligand. In this structrue, the strong anion$\cdots\pi$ interactions between the trapped $[ZnW_{12}O_{40}]^{6-}$ anions and the electron-deficient naphthalenic ring centroids and the $\pi\cdots\pi$ interactions between the DPNDI moieties in the solid-state superstructure can promote electron–hole separation and create a short charge transport pathway. NiW-DPNDI was explored in the reaction of oxidation of styrene under thermocatalysis and photocatalysis systems, respectively, which displayed high efficiency and diverse chemselectivity. Under irradiation, benzaldehyde is the main product, while styrene oxide is by-product in the reaction of oxidation of styrene. However, the main product in thermocatalysis is opposite to that in photocatalysis. In addition, because the carbonic anhydrase (CA)-mimicking Ni sites and the negative electron-enriched POM are well aligned in the pores, which can activate epoxide and promote the capture and activation of CO_2. Thus, NiW-DPNDI shows good effect for CO_2 cycloaddition reactions at a mild temperature. Moreover, it gave a yield of 78% in one-pot tandem reaction (Scheme 1).

NiW-DPNDI was synthesized by $NiCl_2{\cdot}6H_2O$, DPNDI and $Na_{12}[WZn_3(H_2O)_2(ZnW_9O_{34})_2]{\cdot}46H_2O$ precursor under hydrothermal conditions. Single-crystal structural analysis revealed that NiW-DPNDI crystallizes in a space group *P-1*. The asymmetric unit of NiW-DPNDI consists of a $[H_2ZnW_{12}O_{40}]^{4-}$ unit, a $[Ni_2(DPNDI)_{2.5}(H_2O)_7]^{4+}$ cation, and two free H_2O molecules (Fig. 1a). $[ZnW_{12}O_{40}]^{6-}$ shows the Keggin type structure, which connected with two nickel ions (Ni1 and Ni2) by two terminal oxygen atoms, respectively. The Ni1 ion adopts a distorted octahedral geometry and coordinates with one terminal oxygen atoms, one N atom of DPNDI and four H_2O molecules. And Ni2 ion coordinated with two N atoms of two DPNDI molecules, one terminal oxygen atoms and three H_2O. The lability of the coordinated water molecules and free protons allows NiW-DPNDI to act as both Lewis acid catalyst and Brønsted acid catalyst. Ni1 and Ni2 are linked by DPNDI to form a fragment. The fragments are then stacked in a paralleled pattern by $\pi\cdots\pi$ interactions (about 3.3∼3.4 Å) to form a 3D porous structure (Fig. 1b). The H-type aggregate between the DPNDI moieties in the solid-state superstructure is beneficial for enhanced electron transport. The $[ZnW_{12}O_{40}]^{6-}$ anions are localized on the electron-deficient naphthalenic ring centroid with centroid distance 3.0 Å. Hydrogen bonds were found between the C atoms and the imbedded $[ZnW_{12}O_{40}]^{6-}$ anion with separations between C···O about 3.07∼3.30 Å. With these hydrogen bonds interacted $[ZnW_{12}O_{40}]^{6-}$ anion, the sheets were further stacked in a parallel fashion with both the active sites of the Lewis acid catalysts and the oxidation catalysts aligned in the channels. The accessible empty space of the framework is approximately 232.9 $Å^3$ (5.0%), as calculated from PLATON analysis, suggesting the possibility that the MOF-based material NiW-DPNDI can absorb substrates within its pores [31].

The morphology of NiW-DPNDI was characterized by scanning electron microscopy (SEM), which showed quadrilateral shaped blocks with coarse surfaces. The mapping images of NiW-DPNDI reflected the element distribution (Fig. S2 in Supporting information). In the FTIR spectrum, the peaks at 938−768 cm^{-1} are attributed to $\nu(W{=}O_d)$ and $\nu(W{-}O_b/O_c)$ vibrations of $[ZnW_{12}O_{40}]^{6-}$ (Fig. S3a in Supporting information) [32]. The peaks of 1710−1597 cm^{-1} corresponded to C−H, C=O, N-H stretching vibrations of the DPNDI. Elemental analyses and powder X-ray analysis (PXRD) indicated the pure phase of its bulk sample (Fig. S3b in Supporting information). Thermo-gravimetric analysis (TGA) indicated that there is a weight loss of 3.43% (calcd. 3.77%) from 30 °C to 128 °C, which are corresponding to the loss of two free H_2O molecules and seven coordinated water molecules. From 128 °C to 490 °C, there was a weight loss of 5.10% corresponding to half a DPNDI in the framework (calcd. 5.21%). From 490 °C, the skeleton starts to collapse with loss of two DPNDI. The results proved NiW-DPNDI has good thermal stability that meets most of the prerequisites as an ideal platform for heterogeneous catalysts (Fig. 2a).

TPD−CO_2 (temperature-programmed desorption of CO_2) study on CO_2 sorption was carried out [33]. Generally, the different desorption peaks stand for different bonding strength between the CO_2 and the sorbent. In Fig. 2b, two desorption peaks indicated there are two sorption sites at 194 °C and 392 °C, respectively. As seen, there was a desorption peak at 194 °C, meanwhile, there also exited a weight loss in TGA at the similar temperature. This phenomenon verifed that abundant water molecules in the structure can effectively enhance the adsorption of CO_2. The other desorption peak at 392 °C is corresponding to the skeleton collapses. In order to explore the universality of NiW-DPNDI, it was soaked in a series of solution with pH value of 2, 6 and 10 for 24 h, respectively. The IR spectra of soaked crystals are consistent with that of fresh samples, which proved NiW-DPNDI has the good acid-base stability (Fig. S4 in Supporting information).

The optical properties of NiW-DPNDI were researched with UV–vis diffuse reflectance spectroscopy (DRS). As shown in Fig. 2c, it exists optical absorption showed in UV−vis band from 250 nm to 450 nm, which proved it has good light absorption ability. The band gap (E_g) was calculated to be 2.66 eV by using Kubelka−Munk (KM) method based on Tauc plot [34]. As shown in Mott−Schottky plots, NiW-DPNDI is a typical n-type semiconductor [35]. As can be seen from Fig. 2d, the flat band potential of NiW-DPNDI was estimated to be −1.32 V (*vs.* Ag/AgCl). From the equation $E_{CB} = E(vs.\ Ag/AgCl) + 0.2$ V, the negative position of the lowest unoccupied molecular orbital (LUMO) of NiW-DPNDI is estimated to be −1.12 V (*vs.* NHE). The highest occupied molecular orbital (HOMO) potential value is 1.54 V calculate by the equation of $E_{VB} = E_{CB} + E_g$. According to Nyquist plots, NiW-DPNDI has a minimal charge transfer resistance, which indicated that NiW-DPNDI has higher photochemical activity for electron and hole separation (Fig. 2e). It is obvious that NiW-DPNDI has steady and strong photocurrent response than DPNDI, which in harmony with the result of EIS (Fig. 2f). The result further verified the incorporation of the redox-active DPNDI into POM-based MOF can promote the production of abundant of photogenic electrons.

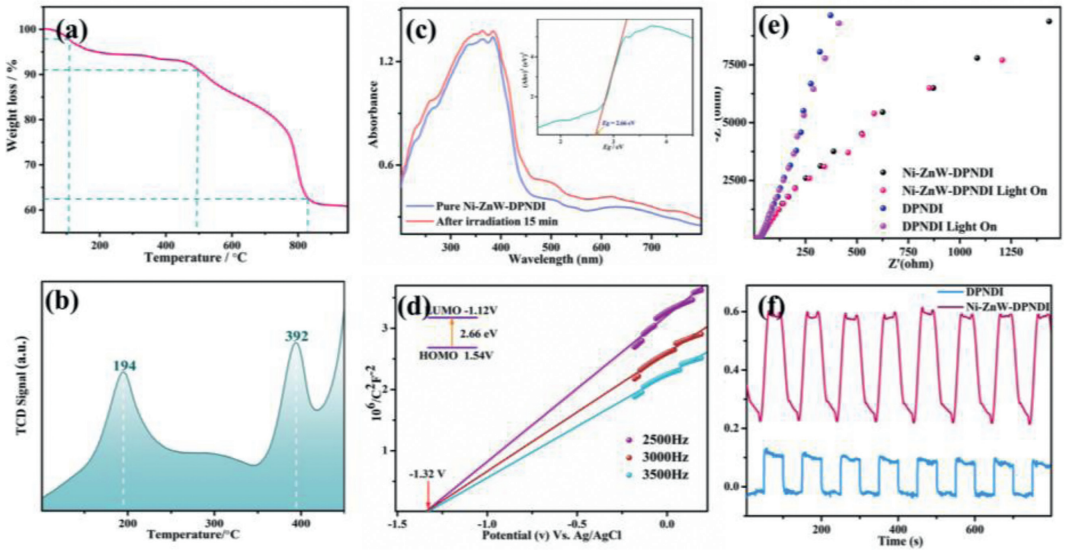

Fig. 2. Characterizations of NiW-DPNDI, (a) TG. (b) TPD−CO_2 curve. (c) Solid UV–vis absorption spectra (inset: Tauc plots). (d) Mott−Schottky plots. (e) Electrochemical impedance spectroscopy (EIS) Nyquist plots in 0.1 mol/L Na_2SO_4 aqueous solution without bias *versus* Ag/AgCl electrode irradiated with white light. (f) Transient photocurrent response in 0.1 mol/L Na_2SO_4 aqueous solution without bias *versus* Ag/AgCl electrode irradiated with white light.

Table 1
Epoxidation of styrene by NiW-DPNDI under thermocatalysis[a] and photocatalysis[b].

Entry	Styrene	Con. (%)[c]	Sel. (%)[c] A	Sel. (%)[c] B
1[a]	Styrene	74.9	95.7	4.37
2[b]	Styrene	79.7	16.3	83.7
3[b]	4-Chlorostyrene	61.5	-	100
4[b]	1-Methoxy-4-vinylbenzene	6.5	-	100
5[b]	4-*tert*-Butylstyrene	3.8	-	100
6[b,d]	Styrene	46.6	-	100
7[b,e]	Styrene	4.8	-	100
8[b,f]	Styrene	1.0	-	100

[a] Thermocatalytic conditions: NiW-DPNDI (20 mg), TBHP (1 mL), CH_3CN (2 mL), 80 °C, 72 h.
[b] Photocatalytic conditions: NiW-DPNDI (20 mg), CH_3CN:CH_3OH (2:1), O_2 (0.1 MPa), 10 W white light, 25 °C, 72 h.
[c] Conversion and selectivity for A and B were determined by ^1H NMR.
[d] With the addition of 1 mL of ·OH capture agent IPA.
[e] With the addition of 20 mg of $^1O_2$ capture agent DABCO.
[f] With the addition of 20 mg of $O_2^{\cdot-}$ capture agent 1,4–benzoquinone.

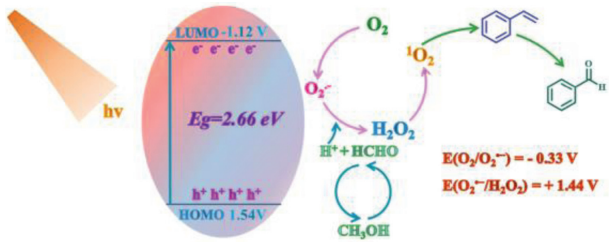

Scheme 2. Proposed catalytic mechanism of photocatalysis of oxidation of styrene.

Table 2
Cycloaddition of CO_2 with epoxides by NiW-DPNDI[a].

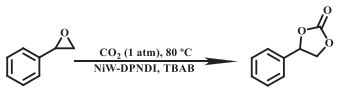

Entry	Epoxide	Yield (%)
1	Styrene oxide	>99
2	Styrene oxide	13.8
3	4-Bromostyrene oxide	93.5
4	Glycidyl phenyl ether	63.5
5	*trans*-Stilbene oxide	5.0
6	Cyclohexene oxide	33.0

[a] Standard conditions: substrate 1 mmol, NiW-DPNDI 20 mg, TBAB 20 mg, CH_3CN 2 mL, CO_2 0.1 MPa, 80 °C, 5 days.

Selective oxidation of styrene was a subject of experimental significance. The photocatalytic reactions were performed on WATTCAS Parallel Light Reactor (WP-TEC-1020HSL) with 10 W 6000–6500 K white LED. In this work, NiW-DPNDI as catalyst were explored in the styrene oxidation under the thermocatalytic and photocatalytic conditions, respectively. We first investigated NiW-DPNDI with *t*-butylhydroperoxide (TBHP, 70% in decane) as the oxidant at 80 °C for 72 h, it gave a 74.9% conversion and 95.7% selectivity for styrene epoxide (Table 1, entry 1). At the same conditions, it gave a 55.75% of conversion and 59.53% selectivity for epoxide without NiW-DPNDI. Combined with the above photoelectrochemical properties, it gave a 66.63% yield of benzaldehyde using O_2 as oxidant under irridiation for 72 h at room temperature. At the same time, there is a 13.02% yield of styrene oxide in photocatalytic reactions (Table 1, entry 2). The blank control experiment gave a 24.20% of conversion and 72.73% selectivity for benzaldehyde. The use of such a catalyst can be extended to the chlorostyrene with comparable activity and selectivity (Table 1, entry 3). However, the substrates with electron-donating groups (as -OCH_3 and -C_4H_9) gave an inferior efficency under the same reaction conditions, which revealed that the substrates are too large to be adsorbed in the channels. It is suggested that the reaction indeed occur in the channels of the POMOF, not on the external surface (Table 1, entries 4 and 5).

A possible reaction mechanism for NiW-DPNDI catalyzed epoxidation of styrene was proposed in Scheme 2. In order to confirm the reactive oxygen species (ROS) contributing to the catalysis, trapping experiments were performed (Table 2, entries 6–8). Isopropanol (IPA) as the ·OH scavenger introduced decreased the conversion from the 79.65% to 46.62%. However, when 1,4-diazabicyclo[2.2.2]octane (DABCO) and benzoquinone were added as $^1O_2$ and $O_2^{\cdot-}$ radical traps, the reactions were almost inert. So

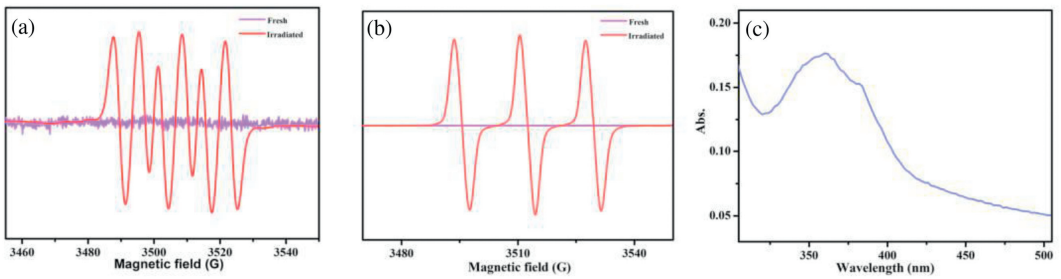

Fig. 3. (a) EPR spectra of $^1O_2$ trapped by TEMPO with O_2. (b) EPR spectra of $O_2^{\cdot-}$ trapped by DMPO. (c) UV–vis absorption spectra of the NiW-DPNDI system after light irradiation for 4 h.

we surmised that $^1O_2$ and $O_2^{\cdot-}$ play major roles in oxidation of styrene under the light. Furthermore, electron paramagnetic resonance (EPR) employing TEMPO and 5,5-dimethylpyrroline-*N*-oxide (DMPO) as the classical $^1O_2$ and $O_2^{\cdot-}$ probes further revealed that both active oxygen species ($^1O_2$ and $O_2^{\cdot-}$) were involved in the photocatalytic reaction (Figs. 3a and b) [36,37]. The formed ROS $O_2^{\cdot-}$ further combined protons that generated from the oxidation of methanol by photogenerated-hole to form H_2O_2 (Fig. 3c), and H_2O_2 further converted into $^1O_2$, which play a supportive role in the oxidation of styrene.

Owing to the excellent CO_2 adsorption and active ability, NiW-DPNDI was also explored to promote the reaction of styrene oxide and CO_2. As a model reaction, the reaction was conducted in CH_3CN under CO_2 atmosphere at 80 °C with an excellent yield of >99% (Table 2, entry 1). The N atoms of DPNDI as basic sites can activate CO_2, and TBAB as nucleophile attacks epoxides to accelerate ring-opening. When the reaction in the absence of TBAB, only a few yield of desired carbonate produced (Table 2, entry 2). When in the absence of NiW-DPNDI, it gave a 65.24% conversion. To demonstrate the catalytic universality of NiW-DPNDI for the reaction with other epoxide substrates under the standard conditions. Compare with the styrene oxide, 2-(4-bromophenyl)oxirane with –Br as electron withdrawing group also showed high conversion (Table 2, entry 3). The lower conversion of trans-stilbene oxide is due to its large steric hindrance impeded the reaction with CO_2 existed in micropores (Table 2, entry 5). Cyclohexene oxide as substrates only obtain 33% yield bacause of high steric hindrance blocked the opening of epoxides (Table 2, entry 6). The stability of NiW-DPNDI plays a critical role in practical use. As shown in Fig. S7a (Supporting information), the XRD peaks intensity of NiW-DPNDI with a slight decrease after 3rd run. The reusability of NiW-DPNDI was investigated in the progress of cycloadditions of CO_2 from styrene oxide, the yield has a little change after 3rd run (Fig. S7b in Supporting information).

We also explored the one-pot tandem catalysis to realize the conversion from styrene to styrene carbonate with NiW-DPNDI as catalyst, TBAB as cocatalyst and TBHP as oxidant under 0.1 MPa CO_2 atmosphere for 5 days at 80 °C, it gave a 78% yield. The experimental result demonstrates catalytic ability of NiW-DPNDI for the one-pot synthesis from styrene to styrene carbonate. In the blank control experiment for cycloaddition of CO_2 from styrene, it gave a 18.6% conversion. Ground on the previous reported mechanism of CO_2 and epoxides activation, a possible reaction mechanism was proposed (Scheme S1 in Supporting information). First, styrene was converted into styrene epoxide with TBHP as oxidant. Next, Ni(II) centers as Lewis acid sites activated ring opening of epoxide to promote interact with the oxygen atom of epoxide. Whereafter, the Br^- of TBAB hit the less blocking of C atoms in the epoxide by nucleophilic attack. Then, combine CO_2 with the active oxygen anions to form alkylcarbonate salts. The final step, styrene carbonate was formed by closing-ring, and NiW-DPNDI was regenerated.

In summary, a new photoactive POMOF NiW-DPNDI was obtained by solvothermal method. The strong anion$\cdots\pi$ interactions between $[ZnW_{12}O_{40}]^{6-}$ anions and the electron-deficient naphthalenic ring centroid and the $\pi\cdots\pi$ interactions between DPNDI moieties promote electron–hole separation and create a short charge transport pathway. NiW-DPNDI gave high efficiency and diverse chemselectivity in the reaction of oxidation of styrene under thermocatalysis and photocatalysis systems. In addition, the carbonic anhydrase-mimicking Ni sites and the negative electron-enriched POM aligned in the pores can activate epoxide and CO_2, thus displaying a good efficiency for cycloadditions of CO_2 with styrene oxide under mild conditions. This work provide a new route for design and construction of excellent solid catalysts and expands the scope of MOFs as heterogeneous photocatalysts.

Declaration of competing interest

The authors declare that they have no known competing financial interests or personal relationships that could have appeared to influence the work reported in this paper.

Acknowledgments

This work was supported by the Natural Science Foundation of Henan (Nos. 202300410043 and 222102230091), the Key Scientific Research Project of Henan Higher Education Institutions (No. 20ZX006), the National Natural Science Foundation of China (No. 21601048).

Supplementary materials

CCDC 2128021 contains the supplementary crystallographic data for this paper. Supplementary material associated with this article can be found, in the online version, at doi:10.1016/j.cclet.2022.107851.

References

[1] C.W.M. Murphy, G.B. Davis, J.L. Rayner, et al., J. Hazard. Mater. 430 (2022) 128482.
[2] Y. Sun, M.Y. Gao, Y. Sun, et al., Inorg. Chem. 60 (2021) 13955–13959.
[3] Q. Lan, S. Jin, B. Yang, et al., Trans. Tianjin Univ. 28 (2022) 214–225.
[4] Z. Wu, S. Guo, L.H. Kong, et al., Chin. J. Catal. 42 (2021) 1790–1797.
[5] Y. Song, Y. Peng, S. Yao, et al., Chin. Chem. Lett. 33 (2022) 1047–1050.
[6] J. Liu, H. Wang, R. Ye, P. Jian, L. Wang, J. Colloid Interface Sci. 585 (2021) 61–71.
[7] Y. Zhang, H. Wang, S. Li, et al., Mol. Catal. 515 (2021) 111940.
[8] K.O. Sulaiman, V. Sudheeshkumar, R.W.J. Scott, RSC Adv. 9 (2019) 28019–28027.
[9] Y. Jiang, Z. Xiong, J. Huang, et al., Chin. Chem. Lett. 33 (2022) 415–423.
[10] Y. Nosaka, A.Y. Nosaka, Chem. Rev. 117 (2017) 11302–11336.
[11] X. Kan, J.C. Wang, Z. Chen, et al., J. Am. Chem. Soc. 144 (2022) 6681–6686.
[12] H. Wang, S. Jiang, W. Shao, et al., J. Am. Chem. Soc. 140 (2018) 3474–3480.
[13] X. Ma, H. Hao, W. Sheng, F. Huang, X. Lang, J. Mater. Chem. A 9 (2021) 2214–2222.
[14] M. Huang, W. Xiang, C. Wang, et al., Chin. Chem. Lett. 31 (2020) 2769–2773.
[15] X. Xiao, M. Lu, J. Nan, et al., Appl. Catal. B 218 (2017) 398–408.
[16] H. Li, S. Yao, H.L. Wu, et al., Appl. Catal. B 224 (2018) 46–52.

[17] M.T.C. Martins-Costa, J.M. Anglada, J.S. Francisco, M.F. Ruiz-López, Chem. Sci. 13 (2022) 2624–2631.
[18] Q. Wang, Q. Chen, G. Jiang, et al., Chin. Chem. Lett. 30 (2019) 1965–1968.
[19] Q. Chen, G.S. Luo, Y.J. Wang, Green Chem. 23 (2021) 7074–7083.
[20] J. Amaro-Gahete, M.V. Pavliuk, H. Tian, et al., Coord. Chem. Rev. 448 (2021) 214172.
[21] Y. Liu, R. Lv, S. Sun, et al., Chin. Chem. Lett. 33 (2022) 807–811.
[22] N. Zhang, L. Hong, A. Geng, et al., Chin. Chem. Lett. 29 (2018) 1409–1412.
[23] Z. Xi, K. Wei, Q. Wang, et al., J. Am. Chem. Soc. 143 (2021) 2660–2664.
[24] M. Tan, M. Takeuchi, A. Takai, Chem. Sci. 13 (2022) 4413–4423.
[25] S.K. Keshri, T. Ishizuka, T. Kojima, Y. Matsushita, M. Takeuchi, J. Am. Chem. Soc. 143 (2021) 3238–3244.
[26] Q. Liu, Q. Zhang, W. Shi, et al., Nat. Chem. 14 (2022) 433–440.
[27] D. Hu, X. Song, S. Wu, et al., Chin. J. Catal. 42 (2021) 356–366.
[28] S. Xing, J. Li, G. Niu, et al., Mol. Catal. 458 (2018) 83–88.
[29] Y. Dong, Q. Han, Q. Hu, et al., Appl. Catal. B 293 (2021) 120214.
[30] G. Hu, W. Chang, S. An, B. Qi, Y.F. Song, Chin. Chem. Lett. 33 (2022) 3968–3972.
[31] L.Q. Wei, B.H. Ye, Inorg. Chem. 58 (2019) 4385–4393.
[32] J. Li, J. jiao, J. Chang, M. Li, Q. Han, Inorg. Chem. 60 (2021) 10022–10029.
[33] J. Liang, R.P. Chen, X.Y. Wang, et al., Chem. Sci. 8 (2017) 1570–1575.
[34] R. López, R. Gómez, J. Sol-Gel Sci. Technol. 61 (2012) 1–7.
[35] X.H. Li, M. Antonietti, Chem. Soc. Rev. 42 (2013) 6593.
[36] J. Duan, L. Chen, H. Ji, et al., Chin. Chem. Lett. 33 (2022) 3172–3176.
[37] J. Wang, Z. Wu, H. Shen, G. Wang, Polym. Chem. 8 (2017) 7044–7053.